UNIVERSITY OF SOUTHAMPTON

Accretion Disc Winds Across The Mass Scale

by

James Matthews

A thesis submitted in partial fulfillment for the
degree of Doctor of Philosophy

in the
Faculty Name
Department of Physics & Astronomy

February 2016

Declaration of Authorship

I, James Matthews, declare that this thesis titled, 'THESIS TITLE' and the work presented in it are my own. I confirm that:

- This work was done wholly or mainly while in candidature for a research degree at this University.
- Where any part of this thesis has previously been submitted for a degree or any other qualification at this University or any other institution, this has been clearly stated.
- Where I have consulted the published work of others, this is always clearly attributed.
- Where I have quoted from the work of others, the source is always given. With the exception of such quotations, this thesis is entirely my own work.
- I have acknowledged all main sources of help.
- Where the thesis is based on work done by myself jointly with others, I have made clear exactly what was done by others and what I have contributed myself.

Signed: _____

Date: _____

"Here, on the edge of what we know, in contact with the ocean of the unknown, shines the mystery and the beauty of the world.

And it's breathtaking."

Seven Brief Lessons on Physics, Carlo Rovelli

"Good enough for government work."

Christian Knigge

UNIVERSITY OF SOUTHAMPTON

Abstract

Faculty Name
Department of Physics & Astronomy

Doctor of Philosophy

by James Matthews

The Thesis Abstract is written here (and usually kept to just this page). The page is kept centered vertically so can expand into the blank space above the title too...

Acknowledgements

The acknowledgements and the people to thank go here, don't forget to include your project advisor...

Contents

Chapter 1

Introduction

"And now you're asking, I don't know where to begin"

Mike Vennart, Silent/Transparent

The release of gravitational potential energy as mass falls towards a compact object is the most efficient energetic process in the universe, capable of liberating more rest mass energy than nuclear fusion. This *accretion* process is thought to power the huge radiative engines at the centres of every galaxy – accreting supermassive black holes known as active galactic nuclei (AGN). In addition to AGN, accretion discs are seen in X-ray binaries (XRBs), young-stellar objects (YSOs) and accreting white dwarfs (AWDs). Accretion therefore appears to be a universal process; broadly speaking, the physics is similar whether it is taking place in a $\sim 1\ M_{\odot}$ Neutron Star or White Dwarf system, or a $\sim 10^{10}\ M_{\odot}$ black hole – a *quasar*.

Outflows are ubiquitous in accreting systems. We see collimated radio jets in AGN (REF) and XRBs (REF), and there is even evidence of extended radio emission in AWDs (REF). These radio jets tend to appear in specific accretion states (REF), implying an intrinsic connection to the accretion process. Even more intriguing, in XRBs less collimated, mass-loaded outflows or *winds* are observed in the opposite accretion state, possibly emanating from the accretion disc. Evidence for disc winds is widespread across the mass range, but perhaps the most spectacular indication is the blue-shifted, broad absorption lines (BALs) in the rest-frame ultraviolet (UV) seen in high-state AWDs (REFs) and so-called broad absorption line quasars seen in $20 - 40\%$ of quasars (BALQSOs; REFs).

The astrophysical significance of disc winds extends, quite literally, far beyond the accretion environment. They offer a potential mechanism by which the central accretion

engine can interact with the host galaxy and interstellar medium (REFs). This is often referred to as AGN feedback (REF), and is required in models of galaxy evolution

This thesis is structured as follows. In the remainder of this chapter, I shall describe the different classes of accreting systems and give a history of their study. In chapter 2, I will give the background accretion theory and detail the successes and failures of accretion disc models when compared to observations, before discussing the outflows associated with accretion discs in chapter 3. Chapter 4 outlines the Monte Carlo radiative transfer (MCRT) and photoionization methods I have used in order to investigate the impact of disc winds on the spectra of accreting systems. The science chapters contain three separate submitted papers, in which we investigated the impact of disc winds on the spectra of CVs (Chapter 5), and tested the disc winds quasar unification model (Chapters 6 and 7). In chapter 8, I summarise my findings and their astrophysical significance, and discuss potential avenues for future work.

1.1 Accreting Compact Binaries

1.1.1 Cataclysmic Variables

Cataclysmic variables (CVs) are systems in which a white dwarf accretes matter from a donor star via Roche-lobe overflow. In non-magnetic systems this accretion is mediated by a Keplerian disc around the white dwarf (WD). Nova-like variables (NLs) are a subclass of CVs in which the disc is always in a relatively high-accretion-rate state ($\dot{M} \sim 10^{-8}$ $M_{\odot}$ yr^{-1}). This makes NLs an excellent laboratory for studying the properties of steady-state accretion discs.

1.1.2 X-ray Binaries

X-ray binaries are similar to CVs in structure, except that the compact object is either a neutron star (NS) or black hole (BH). The accretion disc emits in the soft X-rays, and an additional hard X-ray power law is also seen in the spectrum (REFs). This hard component is normally attributed to Compton up-scattering of seed disc photons by some kind of 'corona' of hot electrons close to the BH (REFs).

Although I do not discuss XRBs directly in this thesis, it is instructive to discuss some of their observational appearance as it is instructive for understanding the theory of disc winds, as well as their wider significance. The discovery that XRBs follow similar tracks on a hardness-intensity diagram (REFs) is particularly interesting in this regard,

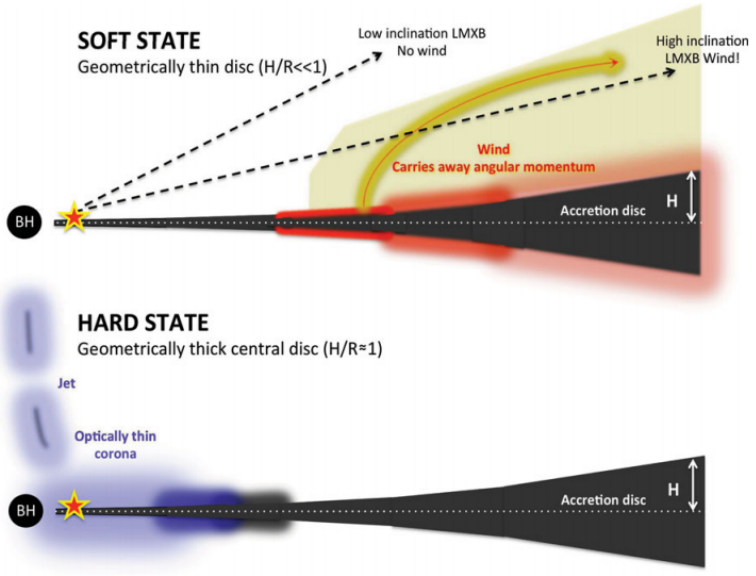

FIGURE 1.1: *Credit: Ponti et al. 2012* Hardness intensity diagram for a WD, NS and BH system

especially since Ponti et al. (2012) showed that broad Fe absorption lines are only seen in the soft-state high-inclination systems, implying that equatorial outflows are intrinsic to the accretion process (see figure 1.1). Although the driving mechanism is almost certainly different to CVs (REFs), the similarity in general structure to models for CVs and quasars is striking.

1.2 Quasars and Active Galactic Nuclei

Spectra of AGN have now been studied for over 100 years, and we have known that they exhibit strong, broad emission lines since the first spectrum was taken by Fath (1909). However, it wasn't until the work of Seyfert (1943) that the systematic classification of AGN really began, leading to the phrase 'Seyfert galaxy'. This label was applied to galaxies possessing a bright nucleus, spectroscopically characterised by a blue continuum and a series of strong emission lines. The first real physical insight into the extraordinary nature of AGN was provided by Woltjer (1959), who noted that (i) the nuclei must have sizes < 100 pc, based on the fact that they were unresolved and (ii) the mass of the nucleus must be very high, based on virialised motion. While both of these observations were based on simple arguments, the fact that these ultra-luminous celestial objects are both *compact* and *supermassive* is perhaps the defining insight into the nature of AGN.

Although the field of AGN study was established in the optical, radio astronomy also significantly furthered our understanding of AGN in the mid-20th century. A number of surveys, such as the Cambridge (Edge et al. 1959), Parkes (Ekers 1969) and Ohio (Ehman

et al. 1970) surveys discovered a great many bright radio point sources distributed isotropically across the sky. These sources eventually became known as 'quasi-stellar radio sources' or *quasars*, and were soon identified to be coincident with bright optical sources or 'quasi-stellar objects' (QSOs; REFs). Nowadays, the term quasar normally has very little to do with radio emission and is often used interchangeably with QSO. Indeed, throughout this thesis I shall refer to a quasar as simply a bright, massive AGN; one with sufficiently high luminosity that it dominates the emission from it's host galaxy.

1.2.1 AGN Unification and the dusty Torus

NGC 1068

1.2.2 The Broad Line Region

1.2.3 Broad Absorption: Evidence of winds

1.2.4 Disc Wind Unification Pictures

As noted by (Murray et al. 1995, hereafter MCGC95), there are a number of problems with the BLR 'cloud' model, perhaps most notably that there is no obvious physical origin for a series of virialised clouds. While there are exceptions to this statement (REFs), it is important to test other models. Indeed, MCGV95 proposed a disc wind model in order to explain both BALs and BELs in quasars. A disc wind model was also discussed by Elvis (2000), who proposed a structure for quasars that attempted to explain much of the behaviour of luminous AGN merely as a function of viewing angle. Outflow models are discussed further in section ?. The philosophy of these models is that, before invoking additional degrees of freedom in a model, we should first test if known quasar phenomenology (winds) can explain other aspects of their observational appearance. I have illustrated this general principle with the 'Occam's quasar' cartoon shown in figure 1.2. This is the picture that I will to test in the latter, quasar-focused sections of this thesis, and the general principle can even be applied to cataclysmic variables and other accreting objects.

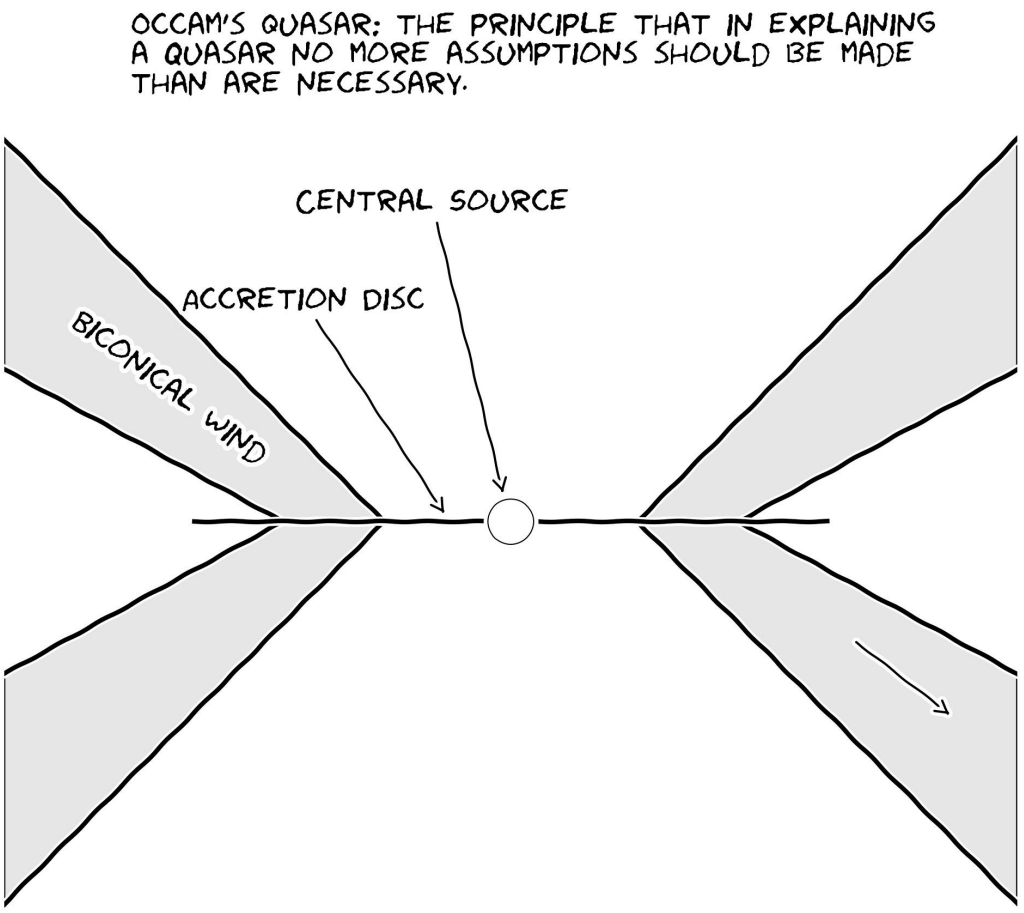

FIGURE 1.2: Occam's quasar. How far can this general picture take us when trying to explain the behaviour of quasars and other accreting compact objects?

Chapter 2

Accretion

As described in the Introduction, there are a wide variety of accreting systems with varying degrees of astrophysical significance. Here I will describe the physics of accretion in more detail, before discussing the theoretical and observational basis for accretion disc winds.

2.1 The Physics of Accretion

The basic phenomenon of accretion- matter falling into a gravitational potential well- is a ubiquitous one in astrophysics.

2.1.1 Roche Lobe-Overflow

In binary systems, there are only two ways by which matter can transfer from the secondary to the compact object. One is by Roche Lobe-overflow (RLOF), whereby stellar evolution causes the donor star to fill it's Roche Lobe, the surface of equipotential around the star. The alternative is that a radiatively driven wind may expel stellar material from the donor, allowing some of it to flow onto the compact object. Although stellar wind accretion is common in some classes (REFs), here I will focus on RLOF as it is more common in the systems that commonly exhibit high-state accretion discs and associated outflows.

The Roche potnetial, Φ_R, can be expressed as ?

2.1.2 Accretion discs

The basic phenomenon of accretion- matter falling into a gravitational potential well- is a ubiquitous one in astrophysics. The details of how and where the energy is released and how angular momentum is transported is subject to a number of different interpretations, mainly depending on the *geometry* of the accretion flow.

The so-called α-disc model developed by (Shakura and Sunyaev 1973, hereafter SS73) is currently the leading candidate for explaining how energy and angular momentum is transported an accretion disc. The starting point for this model is the parameterisation of viscosity using a simple form of

$$\nu = \alpha c_s H. \tag{2.1}$$

Viscous torques then allow the conversion of orbital kinetic energy into heat, which

By considering the energy released through viscous dissipation in the disc it is possible to derive a temperature distribution as a function of radius (Shakura and Sunyaev 1973; Frank et al. 1992).

$$T(R) = \tag{2.2}$$

It is important to recognise that the work of Shakura and Sunyaev (1973) *does not specify the nature of the disc SED*. What it does do is say where energy is originally released. Typically, accretion discs are modelled as a series of annuli each emitting as blackbodies, but it is possible that a disc atmosphere with frequency-dependent opacity would create a somewhat different spectrum. It is also possible that *neither* of these treatments are realistic. We shall therefore devote a little time to discussing the observational arguments for accretion discs and the current problems

2.2 Observational Appearance

2.2.0.1 Potential Problems with the Thin-disc model

A number of issues have been raised with the thin-disc model and its applicability to accreting systems.

2.2.0.2 Quasar emission region sizes from microlensing

2.2.0.3 Quasar emission region sizes from X-ray lags

2.2.0.4 The Spectral shape of CV discs

Attempts to fit the observed SEDs of high-state CVs with simple disc models have met with mixed success. In particular, the SEDs predicted by most stellar/disc atmosphere models are too blue in the UV (Wade 1988; Long et al. 1991, 1994; Knigge et al. 1998a) and exhibit stronger-than-observed Balmer jumps in absorption (Wade 1984; Haug 1987; La Dous 1989; Knigge et al. 1998a). One possible explanation for these problems is that these models fail to capture all of the relevant physics. Indeed, it has been argued that a self-consistent treatment can produce better agreement with observational data (e.g. Shaviv et al. 1991; but see also Idan et al. 2010). However, an alternative explanation, suggested by Knigge et al. (1998b; see also Hassall et al. 1985), is that recombination continuum emission from the base of the disc wind might fill in the disc's Balmer absorption edge and flatten the UV spectrum.

2.3 The Universality of Accretion

Accretion appears to be an important physical processes across ~ 9 orders of magnitude in mass. But is this process the same at all scales? Does any behaviour manifest in all accretion systems?

2.3.1 The RMS-flux relation

Broad-band variability is common in all types of accretion disc. It has been known for sometime that there exists a linear relationship between the flux and absolute root-mean-square (rms) amplitude of this variability. This was discovered first in XRBs and AGN (Uttley and McHardy 2001; Uttley et al. 2005; Heil et al. 2012), but it has been shown more recently that the relationship extends to AWDs and even YSOs (Scaringi et al. 2012, 2015). The relationship is not limited to one type of AWD, as it is present in both NLs and DNe (Van de Sande et al. 2015).

The model that best reproduces this behaviour is the so-called 'fluctuating accretion disc' model (REFs). It has been shown that additive processes cannot reproduce the behaviour, and a multiplicative mechanism is required (REFs). Regardless of the mechanism, the rms-flux relation is one of the most clear-cut examples of a universal accretion

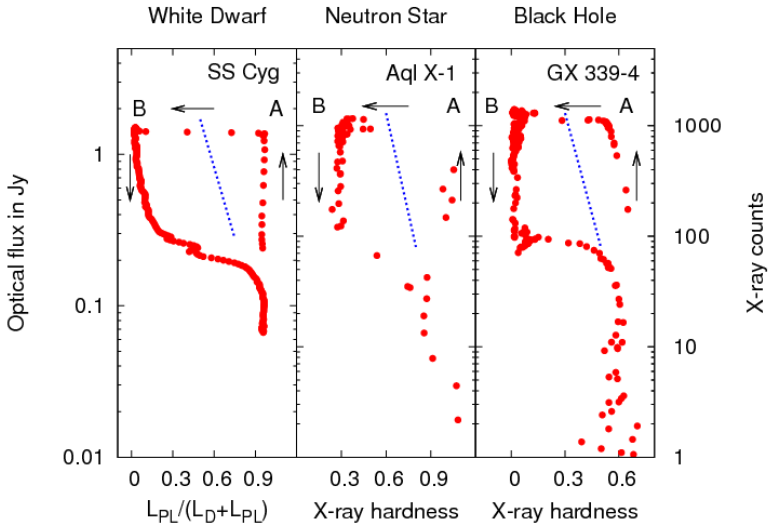

FIGURE 2.1: *Credit: Kording et al. XXXX.* Caption.

phenomenon. It tells us that at least some of the behaviour in AWD discs is present in AGN and XRB, strengthening the argument that AWDs should be used as 'accretion laboratories'.

2.3.2 Accretion States

2.3.3 Jets and Outflows

2.3.4 A Global Picture

Clearly, accretion physics is relevant to a plethora of astrophysical phenomena. It would also appear that the outflowing material observed in accreting systems has a profound effect on the accretion process itself, as well as acting as a spectral 'filter' – modifying, and sometimes dominating the observational appearance of accretion discs.

Chapter 3

Accretion Disc Winds

"A view of space, with an elephant obstructing it"
Mike Vennart, Silent/Transparent

3.1 Accretion Disc Winds: Observational Evidence

3.2 Accretion Disc Winds: Driving Mechanisms

Let us consider a parcel of ideal gas. By imposing nothing more than conservation of mass, energy and momentum on that parcel we can write down three equations of hydrodynamics [1]

$$\frac{D\rho}{Dt} + \rho\nabla \cdot \vec{v} = 0 \tag{3.1}$$

$$\rho\frac{Dv}{Dt} = -\nabla P + \frac{1}{4\pi}(\nabla \times \vec{B}) \times \vec{B} + \rho\vec{F}_{rad} + \rho\vec{g} \tag{3.2}$$

$$\rho\frac{D}{Dt}\left(\frac{e}{\rho}\right) = P\nabla \cdot \vec{v} + \rho\mathcal{L} \tag{3.3}$$

Here D denotes a derivative within the comoving frame of the gas parcel, $\vec{v}$ is the velocity, ρ is the gas density, $\vec{B}$ is the local magnetic field, $\vec{F}_{rad}$ is the radiation force

[1] I stress that these equations are not used in hydrodynamic simulations in this thesis (see section ?, for example); they are discussed here because they provide a natural reference point for exploring potential driving mechanisms for winds in accreting systems.

per unit mass and $\vec{g}$ denotes the gravitational acceleration vector. Equation 3.1 is the *continuity equation* and describes conservation of mass. Equation 3.2 is the *equation of motion* and describes conservation of momentum. Equation 3.3 is the *equation of energy conservation*. We can use equation 3.2 to neatly demonstrate how an outflow can be driven. I have deliberately written the equation so that all the force terms lie on the RHS. We can then see that for an outflow to be driven from an accreting object one simply needs one of the terms on the RHS to dominate over gravity, $\rho\vec{g}$. These terms thus signify three potential driving mechanisms.

- Magnetic Forces, $\frac{1}{4\pi}(\nabla \times \vec{B}) \times \vec{B}$.
- Radiative Forces, $\rho\vec{F}_{rad}$.
- Thermal Pressure, $-\nabla P$.

We can now examine under what physical conditions (and in which corresponding astrophysical objects) we might expect these forces to overcome gravity and cause a parcel of mass to escape to infinity. In other words: *what might drive a wind?*

3.2.1 Thermal Winds

In hydrostatic equilibrium (HSE), thermal pressure balances gravity and no other forces are present, meaning that the equation of motion can be written as

$$\rho\frac{Dv}{Dt} = -\nabla P + \rho\vec{g} = 0 \tag{3.4}$$

Clearly, if the thermal pressure is then significantly increased then this equilibrium condition no longer holds. This can occur in accretion discs at temperatures in excess of $\sim 10^7$ K – where other forces are negligible compared to thermal pressure – and where the escape velocities are relatively low (i.e. far out in the disc). Due to the temperature and gravity scalings, this means that XRBs are natural candidates for showing evidence of thermally driven winds. The outer disc can be heated to the Compton temperature by the central X-ray source, potentially driving relatively high mass-loss rate outflows (Begelman et al. 1983; Woods et al. 1996). This driving mechanism has been proposed as a natural explanation for the ever-present equatorial outflows in soft state XRBs (Ponti et al. 2012). However, they are much less likely candidates in CVs and AGN **Discuss scaling arguments with equations?**.

Chapter 4

Radiative Transfer and Ionization

"I'm splashing greys where once was glowing white"
Mike Vennart, Silent/Transparent

In the previous chapters I have given an introduction to the field and some relevant background relating to accretion discs and their associated outflows. Now it proves useful to discuss some of the specific *methods* one might be able to use in order to answer some of the questions raised in the previous sections. In particular, I will discuss radiative transfer techniques and their potential applications.

4.1 Fundamentals of Radiative Transfer

The most fundamental quantity of radiative transfer is the *specific intensity*, I_ν, defined as

$$I_\nu = \frac{dE}{d\Omega\ dt\ dA\ d\nu}, \tag{4.1}$$

which has units of erg s^{-1} Hz^{-1} sr^{-1} cm^{-2}. By successively multiplying by $\cos\theta$ and integrating over solid angle we can obtain the first and second 'moments' of the radiation field. These are the flux, F_ν and momentum flux, p_ν, respectively, given by

$$F_\nu = \int I_\nu \cos\theta\ d\Omega, \tag{4.2}$$

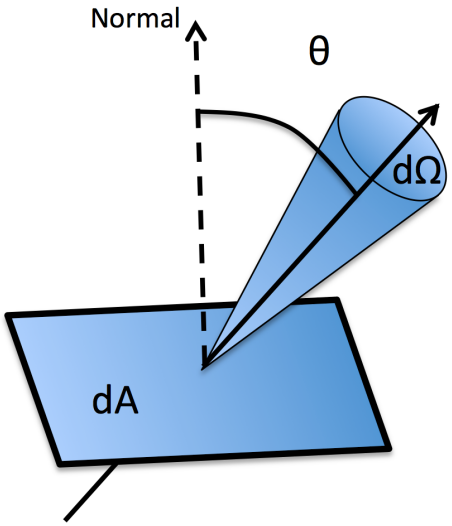

FIGURE 4.1: A schematic showing a ray obliquely incident on a surface of area dA. The labeled quantities are used in the definition of specific intensity.

$$p_\nu = \frac{1}{c} \int I_\nu \cos^2 \theta \; d\Omega \tag{4.3}$$

We can also define the *mean intensity*, J_ν, as

$$J_\nu = \frac{1}{4\pi} \int I_\nu \; d\Omega \tag{4.4}$$

The mean intensity is particularly useful when one wants to ignore the solid angle dependence of the radiation, for example when considering the impact of an ionizing radiation field.

The equation describing the specific intensity change along a path element ds is the radiative transfer equation,

$$\frac{dI_\nu}{ds} = -\kappa_\nu I_\nu + j_\nu, \tag{4.5}$$

where κ_ν and j_ν are the absorption and emission coefficients respectively. If we define the optical depth $d\tau_\nu = \kappa_\nu ds$ we can recast this as

$$\frac{dI_\nu}{d\tau_\nu} = -I_\nu + S_\nu \tag{4.6}$$

where $S_\nu = j_\nu/\kappa_\nu$ is the source function. This equation is called the *formal radiative transfer equation*, and can be solved to give

$$I_\nu = I_{\nu,0}\ e^{-\tau_\nu} + \int_0^{\tau_\nu} S_\nu(\tau'_\nu)\ e^{\tau'_\nu - \tau_\nu} d\tau'_\nu. \tag{4.7}$$

A useful limit is when the source function is constant in the absorbing medium, in which case the integral can be easily evaluated to give

$$I_\nu = I_{\nu,0}\ e^{-\tau_\nu} + S_\nu(1 - e^{-\tau_\nu}). \tag{4.8}$$

4.1.1 Spectral Line Formation

From the above equations, it is trivial to show how emission and absorption lines form when the source function is approximately constant. Say we have a plasma illuminated by a blackbody of temperature T_0, such that $I_{\nu,0} = B_\nu(T_0)$. The plasma layer then has a different temperature, T, such that $S_\nu = B_\nu(T)$ in that medium. By inspecting equation 4.8 we can see that if we are optically thick within the line, but optically thin in the continuum, then inside the line the source term is dominant and outside the line the first $I_{\nu,0}\ e^{-\tau_\nu}$ term dominates. Therefore, if $T > T_0$ we will see an emission line, and if $T < T_0$ we will see an absorption line. This approach describes line emission in the blackbody limit; for more complicated SED shapes it is necessary to construct simple model atoms.

4.1.2 The Two Level Atom

The two level atom formalism is well described by Mihalas (1978).

4.1.2.1 Einstein Coefficients

Within the two level atom, the rate equation between the two levels in LTE can can be written by invoking detailed balance, such that

$$B_{lu}\bar{J}_{ul}n_l = B_{ul}\bar{J}_{ul}n_u + A_{ul}n_u, \tag{4.9}$$

where B_{ul}, B_{2ul} and A_{ul} are the *Einstein coefficients* for absorption, stimulated emission and spontaneous emission respectively. The 'mean intensity in the line', $\bar{J}_{ul}$, is given by

$$\bar{J}_{ul} = \int \phi(\nu) J_\nu d\nu. \tag{4.10}$$

In LTE, the level populations obey Boltzmann statistics, and thus we can also write

$$\frac{n_l}{n_u} = \frac{g_l}{g_u} \exp(h\nu_{ul}/k_B T) \tag{4.11}$$

We can then rearrange equation 4.9 in terms of the mean intensity, and use the fact that, in LTE, $\bar{J}_{ul} = B_\nu(T)$ to write

$$\bar{J}_{ul} = (2h\nu_{ul}^3)/c^2. \tag{4.12}$$

Since this must be true at all values of T we can also show that

$$A_{ul}/B_{ul} = (2h\nu_{ul}^3)\ B_{lu}/B_{ul} = g_u/g_l \tag{4.13}$$

4.1.2.2 Collision Strengths

As well as radiative excitation and de-excitation, bound electrons can also interact with the thermal pool of free electrons, meaning that collisional rates also affect

4.1.3 The Sobolev Approximation

The Sobolev approximation (SA) is a useful limit originally developed. It is used to treat line transfer in fast-moving flows. Originally the theory was mostly applied to Stellar winds, although since then a wide variety of astrophysical objects have been modelled using Sobolev treatments, such as accreting systems (this work) and Supernovae.

The Sobolev limit is when the local bulk velocity gradients in a flow dominate other any thermal broadening. In the presence of these steep velocity gradients, one can assume that the interaction of a ray with a bound-bound transition takes place over a small resonant zone, known as a 'Sobolev surface'. The length of this zone is defined by

$$l_s = \frac{v_{th}}{dv/ds}. \tag{4.14}$$

It is important that the physical conditions of the flow do not change on this scale. If this is the case, then we can assume that all line interactions for a given frequency will occur at a single 'resonant' point. The location at which a given photon will interact with a line of frequency ν_{lu} is then given, in velocity space, by

$$v = c\ \left(\frac{\nu}{\nu_{lu}} + 1\right). \tag{4.15}$$

The Sobolev optical depth is then

$$d\tau = \frac{\pi e^2}{mc}\left(n_l - n_u\frac{g_l}{g_u}\right)\frac{f_{lu}\lambda_{lu}}{c|dv/ds|}. \tag{4.16}$$

We can see that the physical quantities determining line opacity are therefore the level populations in the plasma, the velocity gradient and the atomic physics associated with the bound-bound transition.

4.1.3.1 Escape Probabilities

4.1.4 Monte Carlo approaches

Simple radiation transfer problems can be solved analytically, but with more complicated geometries it is necessary to utilise Monte Carlo techniques, which are easily solved with modern computing approaches and are intuitively parallelisable problems.

4.2 PYTHON: A Monte Carlo Ionization and Radiative Transfer Code

PYTHON[1] is a Monte Carlo ionization and radiative transfer code. The code has already been described extensively by LK02, SDL05 and Higginbottom et al. (2013; hereafter H13), so here we provide only a brief summary of its operation, focusing particularly on new aspects of our implementation of macro-atoms into the code.

4.2.1 Basics

PYTHON operates in three distinct stages, shown in figure 4.2. First, the user specifies the photon sources, geometry and kinematics of the system, normally with a similar parameterisation to the SV93 model described in section **??**. The outflow is then discretised into a logarithmic grid with a user-specified resolution, and the density and velocity in each cell is calculated.

Once the basic setup process has been carried out, the ionization state, level populations and temperature structure are calculated. This is done via an iterative process, by transporting several populations of Monte Carlo energy quanta ('photons' or 'r-packets) through the outflow. This process is repeated until the code converges. In each of

[1]Named c. 1995, predating the inexorable rise of a certain widely used programming language

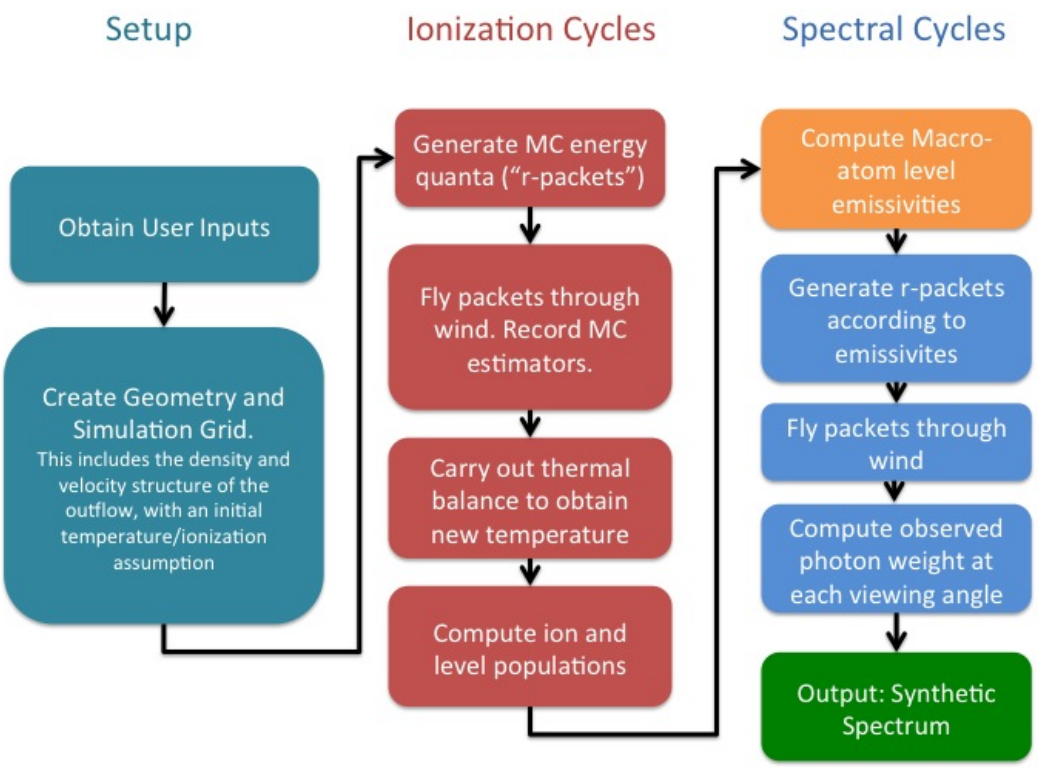

FIGURE 4.2: A flowchart showing the basic operation of PYTHON.

these iterations ('ionization cycles'), the code records estimators that characterize the radiation field in each grid cell. At the end of each ionization cycle, a new electron temperature is calculated that more closely balances heating and cooling in the plasma. The radiative estimators and updated electron temperature are then used to revise the ionization state of the wind, and a new ionization cycle is started. The process is repeated until heating and cooling are balanced throughout the wind.

This converged model as the basis for the second set of iterations ('spectral cycles'), in order to compute the synthetic spectrum based on the MC estimators record during the ionization cycles. The emergent spectrum over the desired spectral range is synthesized by tracking populations of energy packets through the wind and computing the emergent spectra at a number of user-specified viewing angles.

PYTHON is designed to operate in a number of different regimes, both in terms of the scale of the system and in terms of the characteristics of the underlying radiation field. It was originally developed by LK02 in order to model the UV spectra of CVs with a simple biconical disc wind model. SDL05 used the code to model Brackett and Pfund line profiles of H in young-stellar objects (YSOs). As part of this effort, they implemented a 'macro-atom' mode (see below) in order to correctly treat H recombination lines with PYTHON. Finally, H13 used PYTHON to model broad absorption line (BAL) QSOs. For

this application, an improved treatment of ionization was implemented, so that the code is now capable of dealing with arbitrary photo-ionizing SEDs, including non-thermal and multi-component ones.

4.3 Macro-atoms

The macro-atom scheme was created by Leon Lucy and is outlined in his 2002/03 papers. It was implemented in PYTHON *by Stuart Sim, initially for the study of recombination lines in YSO (Sim et al. 2005).*

Lucy (2002, 2003; hereafter L02, L03) has shown that it is possible to calculate the emissivity of a gas in statistical equilibrium without approximation for problems with large departures from LTE. His macro-atom scheme allows for all possible transition paths from a given level, dispending with the two-level approximation, and provides a full non-local thermodynamic equilibrium (NLTE) solution for the level populations based on Monte Carlo estimators. The macro-atom technique has already been used to model Wolf-Rayet star winds (Sim 2004), AGN disc winds (Sim et al. 2008; Tatum et al. 2012), supernovae (Kromer and Sim 2009; Kerzendorf and Sim 2014) and YSOs (SDL05). A full description of the approach can be found in L02 and L03.

The fundamental approach here requires somewhat of a philosophical shift. Normally MCRT is described in the most intuitive way- that is, we imagine real photons striking atoms and scattering, or photoionizing and depositing energy in a plasma. With Lucy's scheme one should instead reimagine the MC quanta as a packets of quantised energy flow, and the scheme as a *statistical* one. The amount of time a given energy quanta spends in a specific atomic level or thermal pool is then somewhat analogous to the absolute energy contained therein.

Following L02, let us consider an atomic species interacting with a radiation field. If the quantity ϵ_j represents the ionization plus excitation energy of a level i then the rates at which the level j absorbs and emits radiant energy are given by

$$\dot{A}_j^R = R_{\ell j}\epsilon_{j\ell'} \quad and \quad \dot{E}_i^R = R_{j\ell'}\epsilon_{j\ell'} \quad , \tag{4.17}$$

Where we adopt Lucy's convention in which the subscript ℓ' denotes a summation over all lower states. Similarly, the rates corresponding to *kinetic* energy transport can then be written as

$$\dot{A}_j^C = C_{\ell' j}\epsilon_{j\ell'} \quad \textit{and} \quad \dot{E}_j^C = C_{j\ell'}\epsilon_{j\ell'} \quad , \tag{4.18}$$

If we now impose statistical equilibrium

$$(\mathcal{R}_{\ell' j} - \mathcal{R}_{j\ell}) + (\mathcal{R}_{uj} - \mathcal{R}_{ju}) = 0 \quad . \tag{4.19}$$

we can then obtain

$$\begin{aligned} &\dot{E}_j^R + \dot{E}_j^C + \mathcal{R}_{ju}\epsilon_i + \mathcal{R}_{j\ell}\epsilon_\ell \\ &= \dot{A}_j^R + \dot{A}_j^C + \mathcal{R}_{uj}\epsilon_i + \mathcal{R}_{\ell j}\epsilon_\ell. \end{aligned} \tag{4.20}$$

This equation is the starting point for the macro-atom scheme. It shows that, when assuming only radiative equilibrium, the energy flows through a system depend only on the transition probabilities and atomic physics associated with the levels the energy flow interacts with. By quantising this energy flow into radiant (r-) and kinetic (k-) packets, we can simulate the energy transport through a plasma discretised into volume elements ("macro-atoms"), whose associated transition probabilities govern the interaction of radiant and kinetic energy with the ionization and excitation energy associated with the ions of the plasma.

Although equation 4.20 assumes strict radiative equilbrium, it is trivial to adjust it to include non-radiative source and sink terms. For example, in an expanding parcel of plasma, adiabatic cooling may be included with a simple modification to the RHS of equation 4.20.

4.3.1 Macro-Atom Estimators

4.3.1.1 Radiation Field Estimators

One of the most important estimators is the 'mean intensity in the line', $\bar{J}_{lu}$, which is defined by equation 4.10.

4.3.1.2 Heating And Cooling Estimators

4.3.2 Ionization Fractions and Level Populations

4.4 Simple-atoms

4.5 Heating And Cooling

4.5.1 Heating And Cooling Balance

4.5.2 Heating And Cooling Estimators

Here I've tried to use Lucy's notation for macro-atom estimators. Take a three level system, in which l and u represent lower and upper levels, and κ represents the continuum level or upper ion. q is the 'absorption fraction' derived below, and q_{ul} and q_{lu} are the collisional rate coefficients.

4.5.2.1 Macro-atoms

In the macro-atom approach, we basically treat two communication pathways. bound-free transitions represent a way for radiant energy to communicate with the thermal pool and bound-bound transitions represent a way for excitation energy to communicate with the thermal pool.

The heating and cooling rates for macro-atom bound-bound transitions are the rates of collisional excitations and de-excitations - i.e. the rate at which thermal energy is converted into bound-bound excitation energy and vice versa.

$$C_{bb,matoms} = \sum_{lines} q_{lu} n_l n_e h\nu_{ul} V \tag{4.21}$$

$$H_{bb,matoms} = \sum_{lines} q_{ul} n_u n_e h\nu_{ul} V \tag{4.22}$$

For bound-free transitions, we define the normal photoionization and recombination rate coefficients γ and α, where α includes stimulated recombination as we do in the code. Note this differs to the approach in Lucy (2003), where it is instead included as a negative photoionization term, hence the notation $\widetilde{\gamma}$. We also need to define two 'modified rate

coefficients' which are the rates at which b-f transitions add and remove energy to the radiation field. These are denoted γ^E and α^E.

The rate at which recombinations convert thermal *and* ionization energy into radiant energy is then $\alpha^E h\nu_{\kappa l} n_\kappa n_e$, where $h\nu_{\kappa l}$ is the potential of the b-f transition, or the energy difference between continuum κ and the level l we are recombining too. The amount of this energy which is removed from the actual thermal pool therefore needs a quantity $\alpha h\nu_{\kappa l} n_\kappa n_e$ subtracted from it, giving

$$C_{bf,matoms} = \sum_{bfjumps} (\alpha^E - \alpha) n_e n_\kappa \nu_{\kappa l} V \tag{4.23}$$

where here I have also included stimulated recombination as we do in the code. Note this differs to the approach in Lucy (2003), where it is instead included as a negative photoionization term, hence the notation $\widetilde{\gamma}$. For photoionizations, we write a similar expression. The rate of at which a level l absorbs energy by b-f transitions is given by $\gamma^E h\nu_{\kappa l} n_\kappa n_e$, but the amount $\gamma h\nu_{\kappa l} n_l$ goes into ionization energy, giving

$$H_{bf,matoms} = \sum_{bfjumps} (\gamma^E - \gamma) n_l h\nu_{\kappa l} V \tag{4.24}$$

as the rate at which radiant energy heats the plasma via b-f transitions.

4.5.2.2 Simple-atoms

In simple-ions it is in some ways a little more complicated. First we define q which will be different for each b-b transition, following Nick's thesis, which is given by (NB: I don't actually know how to derive this)

$$q = \frac{q_{ul} n_e (1 - e^{-h\nu/kT_e})}{\beta_{ul} A_{ul} + q_{ul} n_e (1 - e^{-h\nu/kT_e})} \tag{4.25}$$

where β_{ul} is the angle-averaged escape probability. q represents *the probability that an excited bound electron will collisionally de-excite.* Our b-b heating rate is computed during the photon propagation and is a sum over photons which come into resonance with each line, given by

$$H_{bb,simple} = \sum_{photons} \sum_{lines} (1 - q)(1 - e^{-\tau_S}) w_{photon} \tag{4.26}$$

And our bound bound cooling rate is given by

$$C_{bb,simple} = \sum_{lines} q \left(n_l \frac{g_u}{g_l} - n_u \right) q_{ul} n_e \frac{(1 - e^{-h\nu/kT_e})}{(e^{h\nu/kT_e} - 1)} h\nu_{ul} \tag{4.27}$$

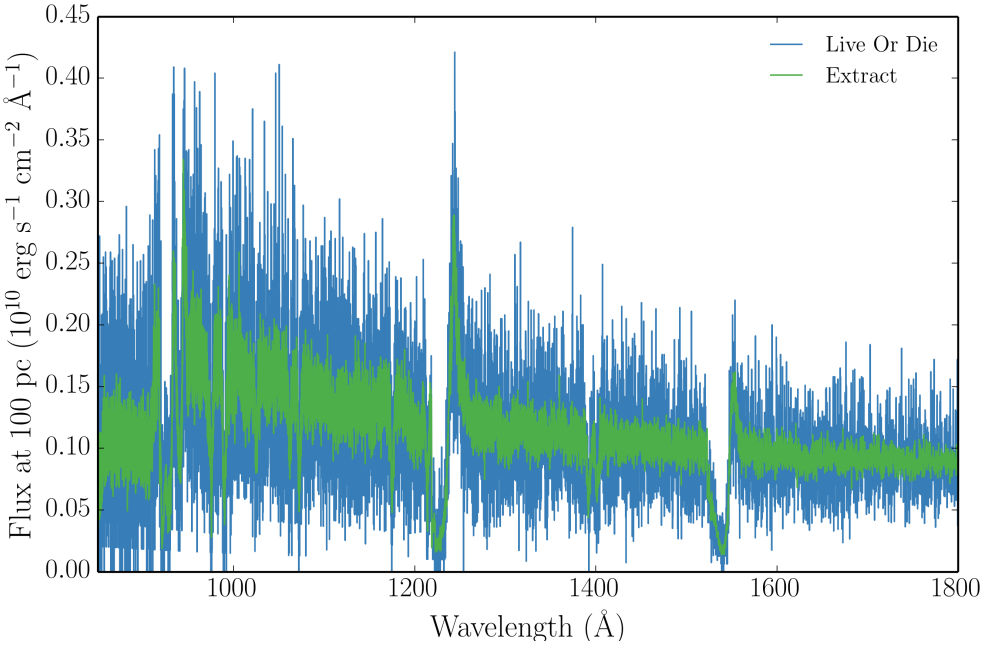

FIGURE 4.3: A Synthetic spectrum after 30 spectral cycles with 100,000 photons from simple CV wind model at a 60° viewing angle. Spectra produced with both the extract and live or die modes are shown. The effectiveness of the extract variance reduction technique can be clearly seen, and we can see that the spectral shape is unaltered.

The bound-free heating rate is given by

$$H_{bf,simple} = \sum_{photons} \sum_{bf\,jumps} w_{photon} e^{-\tau} \frac{\nu - \nu_0}{\nu} \tag{4.28}$$

where ν here is the frequency of the photon in question, and ν_0. The bound-free cooling rate is then

$$C_{bf,simple} = ?? \tag{4.29}$$

4.6 Spectral Synthesis

The primary output from PYTHON is a synthetic spectrum across a range of viewing angles. The code utilises a variance reduction technique in order to minimise the amount of time spent in the portion of the code. This technique is based on a similar method implemented by (Woods 1991).

A comparison between the two methods is shown in figure 4.3.

4.7 Atomic Data

One of the big challenges in building reliable photoionization and radiative transfer lies in the acquisition of accurate and complete atomic datasets. All of the rates described so far contain a term, such as the oscillator strength or dimensionless collision strength, that is dependent purely on the atomic physics associated with the transition. These quantities can be measured in laboratory experiments, or predicted from atomic structure codes which derive the atomic physics from quantum theory.

Photoionization cross-sections are obtained from two sources. Where possible, we use TOPBASE photoionization cross-sections. For macro-atoms, these cross-sections are partial and represent the cross-section for a photoionization from a given *level*. We neglect photoionizations to excited configurations of the upper ion. For simple-atoms they are from the ground state. The TOPBASE cross-sections have two major drawbacks in that

4.8 Clumping

4.8.1 Motivation

As described in section ??, observational evidence for inhomogeneities in outflows is widespread. Clumping a plasma can have a significant effect on its ionization, emission and absorption characteristics. Clearly, the interplay between these effects will be somewhat complex

A number of different implementations of clumping have been explored in previous studies, mostly in the stellar winds community. Perhaps the simplest method is when one assumes that the individual clumps are both optically and geometrically thin; this is known as *microclumping* (e.g. Hamann and Koesterke 1998; Hillier and Miller 1999; Hamann et al. 2008). This technique has been particularly successful in reconciling discrepant mass-loss estimates. It was found that one would obtain different mass-loss rates depending on whether they were calculated from (i) UV resonance scattering of continuum photons (which scales linearly with density; a 'ρ-diagnostic') or (ii) recombination and free-free emission process (which scale with the square of density; 'ρ^2-diagnostics'). A clumped outflow would have enhanced densities in certain regions, and would thus mean that ρ^2-diagnostics tend to overestimate the total mass-loss rates. Microclumping has helped verify this hypothesis with radiative transfer modelling (REFs). These clumpy models also provide better fits to the electron scattering wings of emission lines in stellar winds (**?**).

The second-generation of stellar wind codes went on step further by addressing the issue of *porosity*; that clumps will have a finite size, and thus gaps between the clumps may affect the emergent radiation field. This approach is known as *macroclumping*. **Describe macroclumping with references.**

Implementing a treatment of clumping in accretion disc wind models is challenging, for two main reasons. First, the physical scale lengths and density contrasts in disc winds are not well-constrained from observations, especially in AGN. Second, there are significant computational difficulties associated with adequately resolving and realistically modelling a series of small scale, high density regions with a MCRT code. Given the lack of knowledge about the actual type of clumping, we encorporated the simpler microclumping approach into our code. This is partly because our primary concern was the ionization and emission characteristics of the flow, and porosity was a secondary concern.

4.8.2 Microclumping

To take account of clumping in our outflow we adopt a simple parameterization used in stellar wind modelling. The key assumption here is that typical clump sizes are much smaller than the typical photon mean free path, and thus the clumps are both geometrically and optically thin. This approach is typically known as microclumping and allows one to introduce a 'filling factor', f, which is the fraction of the volume of the plasma filled by clumps. We can then introduce the 'density enhancement', D, which is simply

$$D = \frac{1}{f} \tag{4.30}$$

The densities in the model are then multiplied by this factor. This has the effect of enhancing 'ρ^2' processes such as recombination or collisional excitation, and

4.9 Code Validation

Appendix A

The Effect of Bound-bound Collisional Coefficients on Thermal Conditions of the benchmark CV model

Lorem ipsum dolor sit amet, consectetur adipiscing elit. Vivamus at pulvinar nisi. Phasellus hendrerit, diam placerat interdum iaculis, mauris justo cursus risus, in viverra purus eros at ligula. Ut metus justo, consequat a tristique posuere, laoreet nec nibh. Etiam et scelerisque mauris. Phasellus vel massa magna. Ut non neque id tortor pharetra bibendum vitae sit amet nisi. Duis nec quam quam, sed euismod justo. Pellentesque eu tellus vitae ante tempus malesuada. Nunc accumsan, quam in congue consequat, lectus lectus dapibus erat, id aliquet urna neque at massa. Nulla facilisi. Morbi ullamcorper eleifend posuere. Donec libero leo, faucibus nec bibendum at, mattis et urna. Proin consectetur, nunc ut imperdiet lobortis, magna neque tincidunt lectus, id iaculis nisi justo id nibh. Pellentesque vel sem in erat vulputate faucibus molestie ut lorem.

Quisque tristique urna in lorem laoreet at laoreet quam congue. Donec dolor turpis, blandit non imperdiet aliquet, blandit et felis. In lorem nisi, pretium sit amet vestibulum sed, tempus et sem. Proin non ante turpis. Nulla imperdiet fringilla convallis. Vivamus vel bibendum nisl. Pellentesque justo lectus, molestie vel luctus sed, lobortis in libero. Nulla facilisi. Aliquam erat volutpat. Suspendisse vitae nunc nunc. Sed aliquet est suscipit sapien rhoncus non adipiscing nibh consequat. Aliquam metus urna, faucibus eu vulputate non, luctus eu justo.

Donec urna leo, vulputate vitae porta eu, vehicula blandit libero. Phasellus eget massa et leo condimentum mollis. Nullam molestie, justo at pellentesque vulputate, sapien velit ornare diam, nec gravida lacus augue non diam. Integer mattis lacus id libero ultrices sit amet mollis neque molestie. Integer ut leo eget mi volutpat congue. Vivamus sodales, turpis id venenatis placerat, tellus purus adipiscing magna, eu aliquam nibh dolor id nibh. Pellentesque habitant morbi tristique senectus et netus et malesuada fames ac turpis egestas. Sed cursus convallis quam nec vehicula. Sed vulputate neque eget odio fringilla ac sodales urna feugiat.

Phasellus nisi quam, volutpat non ullamcorper eget, congue fringilla leo. Cras et erat et nibh placerat commodo id ornare est. Nulla facilisi. Aenean pulvinar scelerisque eros eget interdum. Nunc pulvinar magna ut felis varius in hendrerit dolor accumsan. Nunc pellentesque magna quis magna bibendum non laoreet erat tincidunt. Nulla facilisi.

Duis eget massa sem, gravida interdum ipsum. Nulla nunc nisl, hendrerit sit amet commodo vel, varius id tellus. Lorem ipsum dolor sit amet, consectetur adipiscing elit. Nunc ac dolor est. Suspendisse ultrices tincidunt metus eget accumsan. Nullam facilisis, justo vitae convallis sollicitudin, eros augue malesuada metus, nec sagittis diam nibh ut sapien. Duis blandit lectus vitae lorem aliquam nec euismod nisi volutpat. Vestibulum ornare dictum tortor, at faucibus justo tempor non. Nulla facilisi. Cras non massa nunc, eget euismod purus. Nunc metus ipsum, euismod a consectetur vel, hendrerit nec nunc.

Bibliography

Begelman, M. C., C. F. McKee, and G. A. Shields

1983. Compton heated winds and coronae above accretion disks. I Dynamics. *ApJ*, 271:70–88.

Edge, D. O., J. R. Shakeshaft, W. B. McAdam, J. E. Baldwin, and S. Archer

1959. A survey of radio sources at a frequency of 159 Mc/s. *MmRA*, 68:37–60.

Ehman, J. R., R. S. Dixon, and J. D. Kraus

1970. The Ohio survey between declinations of 0 and 36 south. *AJ*, 75:351–506.

Ekers, J. A.

1969. The Parkes catalogue of radio sources, declination zone +20 to -90 . *Australian Journal of Physics Astrophysical Supplement*, 7.

Elvis, M.

2000. A Structure for Quasars. *ApJ*, 545:63–76.

Fath, E. A.

1909. The spectra of some spiral nebulae and globular star clusters. *Lick Observatory Bulletin*, 5:71–77.

Frank, J., A. King, and D. Raine

1992. *Accretion power in astrophysics.*

Hamann, W.-R. and L. Koesterke

1998. Spectrum formation in clumped stellar winds: consequences for the analyses of Wolf-Rayet spectra. *A&A*, 335:1003–1008.

Hamann, W.-R., L. M. Oskinova, and A. Feldmeier

2008. Spectrum formation in clumpy stellar winds. In *Clumping in Hot-Star Winds*, W.-R. Hamann, A. Feldmeier, and L. M. Oskinova, eds., P. 75.

Hassall, B. J. M.

1985. A superoutburst of the dwarf nova EK Trianguli Australis. *MNRAS*, 216:335–352.

Haug, K.

1987. Continuum distributions and line profiles of UX UMA-type novalike systems. *AP&SS*, 130:91–102.

Heil, L. M., S. Vaughan, and P. Uttley

2012. The ubiquity of the rms-flux relation in black hole X-ray binaries. *MNRAS*, 422:2620–2631.

Hillier, D. J. and D. L. Miller

1999. Constraints on the Evolution of Massive Stars through Spectral Analysis. I. The WC5 Star HD 165763. *ApJ*, 519:354–371.

Idan, I., J.-P. Lasota, J.-M. Hameury, and G. Shaviv

2010. Accretion-disc model spectra for dwarf-nova stars. *A&A*, 519:A117.

Kerzendorf, W. E. and S. A. Sim

2014. A spectral synthesis code for rapid modelling of supernovae. *MNRAS*, 440:387–404.

Knigge, C., K. S. Long, R. A. Wade, R. Baptista, K. Horne, I. Hubeny, and R. G. M. Rutten

1998a. Hubble Space Telescope Eclipse Observations of the Nova-like Cataclysmic Variable UX Ursae Majoris. *ApJ*, 499:414–428.

Knigge, C., K. S. Long, R. A. Wade, R. Baptista, K. Horne, I. Hubeny, and R. G. M. Rutten

1998b. Hubble Space Telescope Eclipse Observations of the Nova-like Cataclysmic Variable UX Ursae Majoris. *ApJ*, 499:414.

Kromer, M. and S. A. Sim

2009. Time-dependent three-dimensional spectrum synthesis for Type Ia supernovae. *MNRAS*, 398:1809–1826.

La Dous, C.

1989. On the Balmer jump in dwarf novae during the outburst. *MNRAS*, 238:935–943.

Long, K. S., W. P. Blair, A. F. Davidsen, C. W. Bowers, W. V. D. Dixon, S. T. Durrance, P. D. Feldman, R. C. Henry, G. A. Kriss, J. W. Kruk, H. W. Moos, O. Vancura, H. C. Ferguson, and R. A. Kimble

1991. Spectroscopy of Z Camelopardalis in outburst with the Hopkins Ultraviolet Telescope. *ApJ Letters*, 381:L25–L29.

Long, K. S., R. A. Wade, W. P. Blair, A. F. Davidsen, and I. Hubeny

1994. Observations of the bright novalike variable IX Velorum with the Hopkins Ultraviolet Telescope. *ApJ*, 426:704–715.

Lucy, L. B.
2002. Monte Carlo transition probabilities. *A&A*, 384:725–735.

Lucy, L. B.
2003. Monte Carlo transition probabilities. II. *A&A*, 403:261–275.

Murray, N., J. Chiang, S. A. Grossman, and G. M. Voit
1995. Accretion Disk Winds from Active Galactic Nuclei. *ApJ*, 451:498.

Ponti, G., R. P. Fender, M. C. Begelman, R. J. H. Dunn, J. Neilsen, and M. Coriat
2012. Ubiquitous equatorial accretion disc winds in black hole soft states. *MNRAS*, 422:L11.

Scaringi, S., E. Körding, P. Uttley, C. Knigge, P. J. Groot, and M. Still
2012. The universal nature of accretion-induced variability: the rms-flux relation in an accreting white dwarf. *MNRAS*, 421:2854–2860.

Scaringi, S., T. J. Maccarone, E. Koerding, C. Knigge, S. Vaughan, T. R. Marsh, E. Aranzana, V. Dhillon, and S. C. C. Barros
2015. Accretion-induced variability links young stellar objects, white dwarfs, and black holes. *ArXiv e-prints*.

Seyfert, C. K.
1943. Nuclear Emission in Spiral Nebulae. *ApJ*, 97:28.

Shakura, N. I. and R. A. Sunyaev
1973. Black holes in binary systems. Observational appearance. *A&A*, 24:337–355.

Shaviv, G. and R. Wehrse
1991. Continuous energy distributions of accretion discs. *A&A*, 251:117–132.

Sim, S. A.
2004. Mass-loss rates for hot luminous stars: the influence of line branching. *MNRAS*, 349:899–908.

Sim, S. A., J. E. Drew, and K. S. Long
2005. Two-dimensional Monte Carlo simulations of HI line formation in massive young stellar object disc winds. *MNRAS*, 363:615–627.

Sim, S. A., K. S. Long, L. Miller, and T. J. Turner
2008. Multidimensional modelling of X-ray spectra for AGN accretion disc outflows. *MNRAS*, 388:611–624.

Tatum, M. M., T. J. Turner, S. A. Sim, L. Miller, J. N. Reeves, A. R. Patrick, and K. S. Long

2012. Modeling the Fe K Line Profiles in Type I Active Galactic Nuclei with a Compton-thick Disk Wind. *ApJ*, 752:94.

Uttley, P. and I. M. McHardy

2001. The flux-dependent amplitude of broadband noise variability in X-ray binaries and active galaxies. *MNRAS*, 323:L26–L30.

Uttley, P., I. M. McHardy, and S. Vaughan

2005. Non-linear X-ray variability in X-ray binaries and active galaxies. *MNRAS*, 359:345–362.

Van de Sande, M., S. Scaringi, and C. Knigge

2015. The rms-flux relation in accreting white dwarfs: another nova-like variable and the first dwarf nova. *MNRAS*, 448:2430–2437.

Wade, R. A.

1984. A double grid of accretion disc model spectra for cataclysmic variable stars. *MNRAS*, 208:381–398.

Wade, R. A.

1988. A test of synthetic accretion disk spectra using ultraviolet flux distributions of novalike variables. *ApJ*, 335:394–405.

Woltjer, L.

1959. Emission Nuclei in Galaxies. *ApJ*, 130:38.

Woods, D. T., R. I. Klein, J. I. Castor, C. F. McKee, and J. B. Bell

1996. X-Ray–heated Coronae and Winds from Accretion Disks: Time-dependent Two-dimensional Hydrodynamics with Adaptive Mesh Refinement. *ApJ*, 461:767.

Woods, J. A.

1991. PhD thesis, D. Phil thesis, Univ. Oxford , (1991).